Research papers

A calibration free radiation driven model for estimating actual evapotranspiration of mountain grasslands (CLIME-MG)

D. Gisolo [a], M. Previati [a,*], I. Bevilacqua [a], D. Canone [a], M. Boetti [a], N. Dematteis [a,c], J. Balocco [a], S. Ferrari [a], A. Gentile [a], M. N'sassila [a], B. Heery [a], H. Vereecken [b], S. Ferraris [a]

[a] Interuniversity Department of Regional and Urban Studies and Planning (DIST), Politecnico di Torino and Università di Torino, viale Mattioli 39, 10125 Torino, Italy
[b] Agrosphere (IBG-3), Institute of Bio- and Geosciences, Forschungszentrum Jülich GmbH, 52425 Jülich, Germany
[c] Research Institute for Geo-hydrological Protection, Italian National Research Council, Strada delle Cacce 73, 10135 Torino, Italy

ARTICLE INFO

ABSTRACT

Ecosystems in the Alps are considered hotspots of climate and land use change. In addition, alpine regions are usually characterized by complex morphologies, which make measurement (especially in the long term) of states and fluxes of water, energy and matter particularly challenging. Therefore, there is a limited availability of information and modelling tools to characterize actual ecosystem conditions, and to simulate future scenarios.

Despite the fact that in high altitude areas meteorological forcing is extremely variable in space and time, much of the variability of actual evapotranspiration (*AET*) in the above-mentioned regions is largely related to land surface properties such as aspect, shadowing and slope. Therefore, a simple, radiation driven, calibration free, bucket hydrological model for predicting *AET* and estimating the soil–water balance is proposed here (i.e. CLIME-MG). Conventional meteorological data from a network of automatic weather stations together with a 10 m digital terrain model (aggregated at 30 m), and a land cover map are used to inform the model. All the parameters and values required are obtained or calculated from data provided in literature.

CLIME-MG has proved to perform well for *AET* modelling of mountain grassland. The model is validated both temporally and spatially. Temporal validation of *AET* is performed using eddy-covariance datasets from two different high mountain sites: a sunny and steep abandoned pasture facing S-E at an altitude of 1730 m, and a meadow with a S-SE aspect located at an altitude of 2555 m. Spatial validation is performed by comparing CLIME-MG simulations with the Landsat-based METRIC model evapotranspiration output. Results show good daily temporal performance, especially in wetter periods with recurring rainfall events. Sensitivity of the correlation coefficient between measured and modeled *AET* values to some key parameters such as effective porosity, and the vegetation and stress coefficients was found to be quite low. Spatial validation of hourly results shows SPAEF values in the range 0.21–0.34 between the outputs of the two models (with a similar spatial structure ruled by the DTM). Boxplots of deviations between CLIME and METRIC with respect to morphological characteristics has highlighted some dependency on elevation and slope (but not on aspect and soil depth); this suggests an opportunity to refine the modelisation of the grassland *AET* processes. Finally, spatial results demonstrated the non-sensitivity of the proposed model to local elevation and to the distance from the meteorological stations.

1. Introduction

Starting from the late 19th century, Alps have been subjected to a warming rate which is about two times larger than the northern-hemispheric average (Auer et al., 2007) and it is mainly due to water vapour-enhanced greenhouse warming (Philipona, 2013). Despite the fact that seasonal and spatial patterns of temperature show remarkable variability, all models agree in highlighting this phenomenon making the warming trends very robust (Heinrich et al., 2013b). As annual average, a total increase of about 1.5 °C is expected in the first half of the 21st century (~0.25 °C per decade). A further acceleration is foreseen in the second half of the century with an expected annual average warming at the end of the century of about 3.3 °C (~0.36 °C per decade if only the second half of the 21st century is considered) especially at high elevations - Gobiet et al. (2014). These warming dynamics are influencing

Nomenclature

a_i	Regression parameters, -
AET	Actual evapotranspiration, mm h^{-1}
AWS	Automatic weather station, -
α	Albedo, -
$1/\sin(d)$	Optical depth of the atmosphere, m
β	Slope of the surface, Rad
b_i	Regression parameters, -
c_i	Regression parameters, -
c_p	Air specific heat, J mol^{-1} K^{-1}
d	Relative Earth-Sun distance, m
D	Dew deposition, mm
DTM	Digital Terrain Model, -
Δ	Slope of the saturation vapour pressure curve, kPa K^{-1}
ET	Evapotranspiration, Kg m^{-2} s^{-1}
e_a	Actual vapour pressure, kPa
e_s	Saturation vapour pressure, kPa
ϵ	Gray body emissivity, -
G	Ground heat flux, W m^{-2}
G_{sc}	Solar constant (1367 W m^{-2}), W m^{-2}
γ	Psychrometric constant, kPa K^{-1}
H	Sensible Heat flux, W m^{-2}
H_a	Absolute humidity, g m^{-3}
K	soil diffusion coefficient, m yr^{-1}
K_c	Vegetation coefficient, -
K_s	Vegetation stress coefficient, -
λ	Latent heat of vaporisation, MJ kg^{-1}
LE	Latent Heat flux, W m^{-2}
LW_{in}	Incoming long wave radiation, W m^{-2}
LW_o	Outgoing long wave radiation, W m^{-2}
m	Soil empirical constant, cm^{-1}
n	Number of soil layers, -
P	Precipitation, mm
P_0	Maximum bedrock-soil conversion rate, m yr^{-1}
$Perc$	Percolation, mm
PET	Potential evapotranspiration, mm h^{-1}
q_a	Actual specific humidity, kg kg^{-1}
q_s	Saturation specific humidity, kg kg^{-1}
q_{soil}	Net sediment transport vector, cm^2 yr^{-1}
R_n	Net radiation, W m^{-2}
r_a	Aerodynamic resistance, s m^{-1}
r_s	Surface resistance, s m^{-1}
ρ_{air}	Air density, kg m^{-3}
ρ_{rock}	Rock density, kg m^{-3}
ρ_s	Effective soil porosity, -
ρ_{soil}	Soil density, kg m^{-3}
s	Slope of the saturation specific humidity curve, K^{-1}
σ	Stefan-Boltzmann constant, W m^{-2} K^{-4}
SW_b	Beam radiation, W m^{-2}
SW_d	Diffuse radiation, W m^{-2}
SW_{in}	Incoming shortwave radiation, W m^{-2}
SW_o	Outgoing short-wave radiation, W m^{-2}
SW_{anom}	SW_{in} anomaly, W m^{-2}
T_a	Air temperature, K
T_{day}	Daytime temperature, K
TAW	Total available water, Mm
τ	Transmittance of the atmosphere, -
τ_{sw}	Broadband atmospheric transmissivity, M
θ	Potential temperature, K
θ_{rel}	Solar incidence angle, Rad
W_l	Water available in a layer, Mm
z	Terrain elevation, M
z_l	Layer depth, Mm
z_s	soil depth, M
RH	Relative Humidity, -

(and will increasingly influence) the Alpine Region and, more generally, all mountainous areas (e.g. Palazzi et al., 2017; Rottler et al., 2019). Impacts are already evident. It is changing: i) the physical environment (e.g. increased thaw of permafrost regions, reduced snow-cover at mid-elevation, glacier retreats, increased frequency of drought and water scarcity – Haeberli and Beniston, 1998; Harris et al., 2003; Vanham, 2012; Gobiet et al., 2014; Beniston and Stoffel, 2014); ii) the biodiversity and evolutionary dynamics of the Alpine biosphere (e.g. distribution and abundance of biotic communities, seasonal cycles and phenology modifications – Klanderud and Totland, 2005; Alexander et al., 2015; Rogora et al., 2018; Asse et al., 2018); and iii) its socio-economic implications (e.g. winter tourism and ski industry, hydropower generation, natural hazards, agriculture and irrigation, drinking water, ecosystem services – Gilaberte-Búrdalo et al., 2014; Steiger, 2010, Gaudard et al., 2014; Maran et al., 2014; Einhorn et al., 2015; Fuhrer et al., 2014; Delpla et al., 2009; Schirpke et al., 2017).

Within this context, evapotranspiration is a key variable linking ecosystem functions, carbon and climate feedbacks, agricultural management, and water resources and its accurate determination is one of the main challenges identified for Earth System Science (Fisher et al., 2017). It is a complex process depending on many factors, namely water availability, energy availability, wind speed, humidity gradient, physical attributes of the vegetation (stress included), and soil characteristics. Topography plays a major role. Due to its importance in a wide range of disciplines and contexts, a suite of methods and techniques have been developed to measure or estimate evapotranspiration (e.g. Wang and Dickinson, 2012) using analytical and empirical approaches together with direct or indirect methods.

Firstly we find the experimental surveys at the field scale which use various approaches, namely: hydrological approaches (e.g. weighing lysimeters – Evett et al., 2012, Previati et al., 2020; soil–water balance – Chen et al., 2008, Raffelli et al., 2017); micrometeorological approaches (e.g. eddy covariance – Wever et al., 2002, Gu et al., 2008, Ochoa-Sánchez et al., 2019; aerodynamic methods – Ortega-Farias et al., 1996; energy balance and Bowen ratio – Malek and Bingham, 1993); plant physiology rule-based approaches (e.g. sap flow method – Granier, 1987; chambers systems – Reicosky et al., 1983); and optical approaches (e.g. scintillometry - Hemakumara et al., 2003).

Further methods use meteorological variables and/or remote sensing based estimations. The first group are algorithms that use meteorological variables to estimate actual evapotranspiration starting from reference/potential evapotranspiration. This includes temperature based models (e.g. Thornthwaite, 1948; Blaney & Criddle, 1950; and Hargreaves and Samani, 1982), solar-radiation based models (e.g. Makkink, 1957; Priestley & Taylor, 1972), and "mixed" models which are based on energy/mass balance principles (e.g. Penman, 1948; modified Penman (Doorenbos and Pruitt, 1977); FAO Penman-Monteith (Allen et al., 1998)). The second cluster are solutions that use remote sensed variables and they can be roughly organized in three branches: Methods demanding remotely sensed atmospheric and radiation variables (e.g. Venturini et al., 2008), Methods based on remotely sensed vegetation indexes such as NDVI (where surface losses depend mostly on the intensity of transpiration - e.g. Cleugh et al., 2007), and Methods based on remotely sensed surface temperatures such as thermal infrared domain (i.e. contextual pixel models: based on the simultaneous presence of hot/dry and cold/wet pixels within the satellite image – e.g. S-SEBI (Roerink et al., 2000), TTME (Moran et al., 1994), SEBAL (Bastiaanssen et al., 1998; Bastiaanssen et al., 2005), and METRIC (Allen et al., 2007; De la

Fuente-Sáiz et al., 2017); single pixel models: solving the surface energy budget for each pixel independently from the others – e.g. TSEB (Norman et al., 1995; Chirouze et al., 2013), SEBS (Su, 2002; Sharma et al., 2016)).

For a more comprehensive overview, several reviews are available (e.g. Rana and Katerji, 2000; Li et al., 2009; Wang and Dickinson, 2012).

Alpine regions, being usually characterized by complex environmental and terrain conditions combined with limited accessibility that hampers realization of surveys and studies, suffer from a limited quantity and quality of information as well as the lack of appropriate modelling tools to characterize actual conditions, to make forecasts and envisage scenarios (especially true at local scale where topographic factors can lead to strong changes/gradients influencing the local energy-mass balance - Aguilar et al., 2010).

Satellite observations, together with the above-mentioned remote sensing based approaches, can partially close this lack of information, but they are usually designed for routine applications over large regions, hence characterized by coarse resolutions in space and/or in time (depending on the orbital patterns of the sensor platform and sensor specifications - e.g. Landsat images have a temporal resolution of 16 days and a spatial resolution of 30 m – USGS, 2019). Furthermore, satellite observations can be heavily affected by cloudy conditions and the information retrieved is usually subject to post-processing analysis and calibration procedures which are not often easy-to-apply or user-friendly.

In this context, climate change studies in mountain areas require more and more *AET* models with higher spatial and temporal resolution (Gürtz et al., 2005) to account for the local terrain and ecosystem complexity. These must function without the possibility to rely on the abundance of data that are usually found at lower altitudes. This activity, unfortunately, is still challenging. Considerable efforts have been made both to develop algorithms and models for estimating land surface evaporation (e.g. Carter and Liang, 2018; Bottazzi et al., 2021), and to evaluate the influence of complex morphologies on specific meteorological/environmental variables and/or to implement common modelling applications (e.g. Solar radiation/shading: Duguay, 1995; Kumar et al. 1997; Oliphant et al. 2003; Aguilar et al., 2010). We are not aware of any existing parsimonious calibration free models able to estimate *AET* over complex terrains at high spatial and temporal resolution using only a digital terrain model, a land cover map, and standard meteorological data.

Distributed physically-based land surface models (LSMs) - such as, the Community Land Model (CLM), the Ecological Assimilation of Land and Climate Observation model (EALCO), the Variable Infiltration Capacity model (VIC) - account explicitly for spatially variable properties of watersheds but require parameter values which are not commonly available for complex contexts, and cannot be realistically obtained. For instance, soil parameters can be estimated (or derived) from easily measured variables (i.e. pedotransfer) and used to inform hydrological models (e.g. Baveye and Labac, 2015; Van Looy et al., 2017). But at high altitudes even simple soil characteristics are difficult to obtain. Pedotransfer functions may provide reasonable approximations but only as long as one remains within the particular set of soils for which specific functions have been developed (e.g., Wösten et al., 1990). A similar situation can be acknowledged also for further key properties, such as soil depth (i.e. thickness of unconsolidated material over un-weathered bedrock). These can be estimated, especially over large areas, by three different approaches: (i) physically based models; (ii) empirico-statistical methods using environmental parameter correlation, and (iii) interpolation from sample points (e.g. Sarkar et al., 2013, for a more comprehensive analysis).

In addition, since global climate change has become a popular issue since the late 1980 s, most LSMs were conceived and developed for working at regional (up to global) scale, with large model grids (both in input and in output) resulting in a general smoothing of the local heterogeneity typical of complex systems (e.g. Wang et al., 2015; Zhao & Li,

2015). Due to that, most LSMs have tried to represent the spatial heterogeneity over complex terrains by applying different processing techniques and/or sub-grid systems. CLM, for example, offers the possibility to adopt a three-level sub-grid system to represent the vegetated surface according to a few specified plant functional types. VIC model allows to divide the grid cell in sub-grid elevation bands (with 500 m elevation interval).

To better represent the process interactions between hydrology, ecology, and atmosphere - especially at higher spatial resolution (e.g. catchment scale) -, LSMs have begun to be coupled with hydrological models. These tools, useful for simulating surface/ subsurface processes, are mainly oriented towards integrating and solving the Richards' equation. Among others, CATHY (e.g.Paniconi & Wood, 1993; Niu et al., 2014), ParFlow (e.g. Kollet and Maxwell, 2006) and GeoTOP (Rigon et al., 2006) can be identified as the most known. All these models differ in several aspects such as the Richards' equation solving approach, the spatial discretization, and the flow conceptualization (it is interesting to note that GeoTOP accounts for very complex topography). Complex models can provide a good fit with *AET* measured data (e.g. Fig. 10 of Rigon et al., 2006). However, they require many inputs which are not available in mountainous areas. For example, Mastrotheodoros et al. (2020) paper shows the results of a very detailed model to forecast the effect of climate change in the Alps. Their Tethys-Chloris model was conceived to deal with different kinds of vegetation, and coupling various mechanisms, including carbon balance.

We think that simplified models can be complementary tools to be used in conjunction with such detailed models. Also, simple models can be valuable for real world applications (e.g. Brussolo et al. (2022), where a similar simple model (by the same authors of this paper) was used by a drinking water authority. It must be cited that Filippa et al. (2022) recently studied the productivity of grassland in the same Gran Paradiso area as used by CLIME-MG; however, they took an agronomic point of view, not a modelling one.

In this challenging context, some interesting insight can be found in the following intuitions. Rogowski (1972), in his landmark article on soil spatial variability, identified criteria according to which soils in a watershed could be assumed uniform, i.e., its heterogeneity could be ignored. Also, Bouma (1989) stated that soils that are pedologically different are not necessarily different in their hydrological properties. More recently McDonnell et al. (2007) have pointed out the need to devise a way to embed heterogeneity, or the consequence of heterogeneity, into models in a manner that does not require enormous amounts of generally unavailable data. One way to do this, according to these authors and in resonance with Jury's (1982) perspective, is not to concentrate one's efforts on a detailed characterization of the heterogeneity of the system, but to focus on the "properties that emerge with increasing scales, and on their resulting hydrological effects" (Baveye and Labac, 2015). Some studies (e.g. Basu et al, 2010) found a quite spatially homogeneous soil water storage capacity at the watershed scale.

The objective of this work was to present and validate a new calibration free soil water model (i.e. CLIME-MG) for computing the soil--water balance and mapping the actual evapotranspiration *(AET)*. CLIME-MG is a 1D water balance model (i.e. bucket model) accounting for landscape differences in aspect, topography/morphology, soil depth, and meteorological forcing. It is specifically designed to work at very high spatial and temporal resolutions over grasslands in mountain/complex-morphology domains, and it would act as a magnifying glass to bridge local point data and satellite data at larger scales. The necessary inputs are a digital terrain model (hereafter DTM), a land cover map and standard meteorological data retrieved from the regional network, here referred to as Automatic Weather Stations (AWS). The model is built without calibration parameters, and only literature parameters values are used.

Bearing in mind that nowadays a number of standard automatic meteorological stations provide data at hourly temporal resolution, and

satellite data provide information at a smaller than hillslope scale (i.e. 20/30 m) - but with only few images per growing season -, the here presented results are performed at 1-hour temporal and 30 m spatial resolutions in a 600 km^2 wide area in the Alps, during two growing seasons in two different sites characterized by different conditions and very different average amounts of soil water. Modelled *AET* data during the two growing seasons are compared with eddy covariance measured *AET* data to check the temporal variability, and with Landsat *AET* data computed via METRIC model to check the spatial variability.

2. Materials and methods

2.1. CLIME-MG model structure

The here presented model is composed of two main modules: the meteorological module and the soil–water-balance module. The meteorological module uses meteorological data to compute the potential evapotranspiration *(PET)* with the Penman-Monteith formula following the Allen et al. (1998) approach:

$$PET = \frac{1}{\lambda}\frac{\Delta(R_n - G) + \rho_{air}c_p\frac{e_s - e_a}{r_a}}{\Delta + \gamma\left(1 + \frac{r_s}{r_a}\right)} \tag{1}$$

Notations are reported in the list of symbols at the beginning of the paper.

The soil–water balance module (SWB-module) computes the soil–water balance to estimate the vegetation stress coefficient, K_s, and thus the fraction of water vapour transferred to the atmosphere (and, therefore, the ratio *AET/PET*).

2.1.1. Meteorological module

The CLIME-MG meteorological module spatially interpolates punctual meteorological data provided by meteorological stations. Hourly time-step standard weather data (namely temperature, humidity, global solar radiation, wind, precipitation, air pressure) were averaged starting from existing AWS located in the domain, while other variables were computed using known formulas obtained from literature, as better detailed in the following. The daily values of air temperature, relative humidity and global solar radiation measured at the AWS (Fig. 1) show that the spatial variability of these is limited, and that most of the

variability is temporal. The time series measured at different AWS are generally in phase. Differences between air temperature series are due to elevation (e.g. higher values belong to the AWS located at lower elevation (i.e. Vieyes – Table 1)). Wind and precipitation are more variable in space, hence these variables were averaged in the horizontal direction (e.g. Voronoi approach was adopted for precipitation). When empirical formulas were adopted for estimating variables, parameters belonging to published look-up-tables were used (i.e. most of them are reported in the FAO volume 56, or specified in the following section of the paper).

2.1.1.1. Radiation. To compute the net radiation on the domain, the four solar radiation components were here reconstructed taking into consideration the shading effect. In particular, the hourly SW_{in} was mapped over the whole domain starting from data collected by a representative local station corrected for shading and sloping effects in order to obtain a SW_{in} on a horizontal surface. To this end, and to compute the hours of shading, a model using the DTM topographic information was implemented using TopoToolbox (Schwanghart and Scherler, 2014) together with a set of Matlab functions for topographic analysis.

Beam (SW_b) and diffuse (SW_d) radiation, were separately estimated according to:

$$SW_{in} = SW_b + SW_d \tag{2}$$

The beam radiation incident on a sloping surface, SW_b, is a function of the zenith angle and illumination angle (Iqbal, 1983; Twidell and Weir 1986; Aguilar et al., 2010).

SW_b was calculated as suggested by Chung and Yun (2004).

$$SW_b = SW_{in}\tau^{1/\sin(d)} \tag{3}$$

where d is the atmospheric thickness as a function of the sun position (i. e. elevation). A Rayleigh sky condition and an isotropic sky radiation were also assumed (so SW_d was only affected by the sky view factor: $SVF = \cos^2(\beta/2)$, following Chung and Yun (2004)). A value of $\tau = 0.8$ was used. The actual diffuse radiation collected by a surface with slope SW_d was hence calculated using the equation:

$$SW_{d,\beta} = SW_d SVF \tag{4}$$

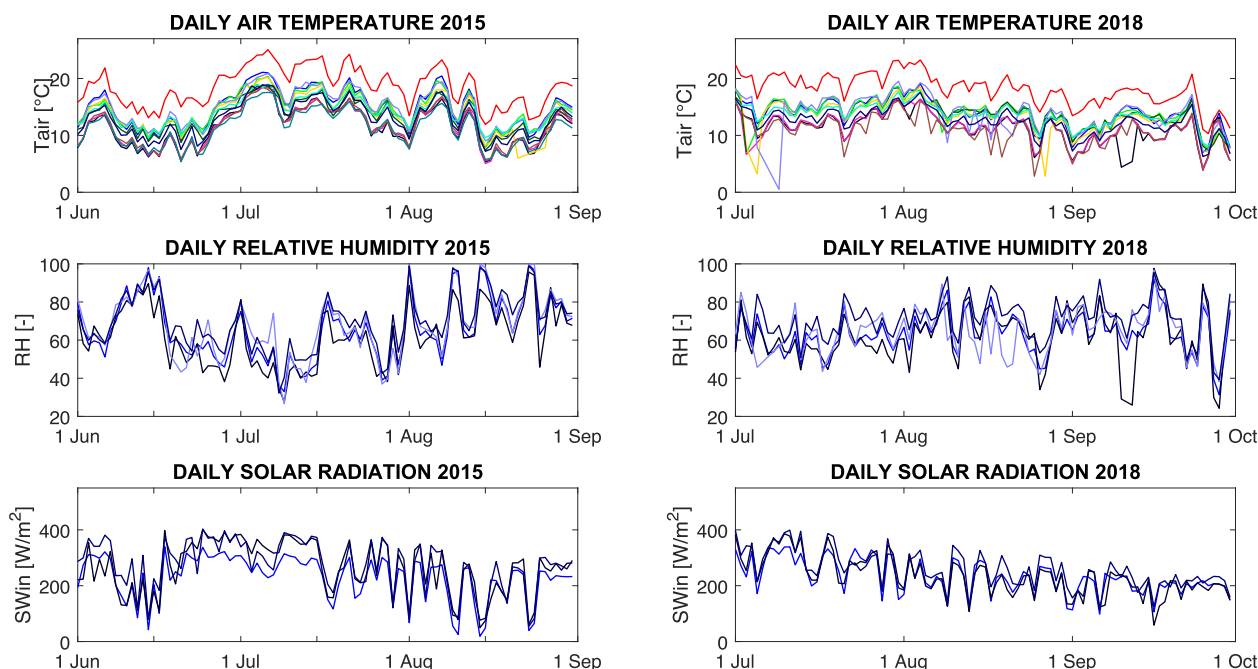**Fig. 1.** Daily values of air temperature (T_a), relative humidity (RH) and solar radiation (SW_{in}) for the 2015 and 2018 growing seasons.

Table 1
Automatic Weather Stations (AWS) variables.

	n	Elevation [m]	$T_a[°C]$	$RH[\%]$	$U_z[m/s]$	$P[mm]$	SW_{in}
Vieyes	1	1139	yes	no	no	yes	no
Lillaz	2	1613	yes	no	no	yes	no
Cogne	3	1785	yes	yes	yes	yes	yes
Gran Crot	4	2279	yes	no	yes	yes	no
Valnontey	5	1682	yes	no	no	yes	no
Cretaz	6	1470	yes	no	no	no	no
Clavalité	7	1531	yes	yes	yes	yes	no
Lavodilec	8	2250	yes	no	no	yes	no
Gressan	9	2280	yes	yes	yes	yes	yes
Eaux Rousses	10	1651	yes	no	no	yes	no
Orvieille	11	2170	yes	no	no	yes	no
Pont	12	1951	yes	yes	yes	yes	yes

Outgoing radiation was computed as $SW_o = \alpha SW_{in}$. For grasslands, typical values of albedo vary between 0.15 and 0.23 (Brutsaert, 2005). In the model the albedo was set to $\alpha = 0.17$.

LW_{in} and LW_o were computed with the Stefan-Boltzmann law. For LW_{in}, the emissivity was parametrized as (Brutsaert, 2005):

$$\epsilon = a\left(\frac{e_a}{T_a}\right)^b = 0.99 \tag{5}$$

where the coefficients introduced by Brutsaert (2005) were used, namely $a = 1.24$, and $b = \frac{1}{7}$.

For LW_o, the surface temperature was estimated with a linear relationship with T_a, as reported by Gallo et al. (2011) and Jin and Mullens (2014):

$$LW_0 = \epsilon\sigma(T_s)^4 \tag{6}$$

The soil surface temperature is given by $T_s = c_o + c_1 T_a$. A discrimination between night and day was used. Averaged values for daytime during clear and cloudy conditions were taken from Gallo et al. (2011): $c_0 = -2.075°C$ and $c_1 = 1.075$. At night, the situation was supposed to be different. Following the findings of Jin and Mullens (2014), we assumed this difference as a constant during the night-time hours. Therefore, $T_s = T_a - 1.5$. This approximation relies on the absence of strong fluctuations of the two temperatures during night-time.

2.1.1.2. Air temperature. Two different approaches were followed for mapping daytime and night-time temperatures. During the day, in complex terrains, air temperature is primarily affected by solar radiation and elevation. Available solar radiation, in turn, is governed by shading due to the surrounding mountains (Chung and Yun, 2004). Therefore, topography plays an important role in the spatial distribution of the air temperature. To estimate daytime temperature (T_{day}) a multi-linear regression was adopted:

$$T_{day}(z, SW_{anom}) = a_0 + a_1 z + a_2 SW_{anom} \tag{7}$$

where SW_{anom} is the difference of SW_{in} of a given location with respect to the spatial average across the considered domain, with $a_2 \geq 0$.

For night-time, after sunset, temperature inversion occurs in a stable atmosphere. Thus, it was simpler to reconstruct the potential temperature (θ), with a vertical profile in free atmosphere approximated by the formula (from Stull, 1988):

$$\theta(z) = b_0 - b_1 e^{-z/b_2} \tag{8}$$

To this purpose, Whiteman et al. (2004) and Massaro et al. (2015) observed that the pseudo-vertical profile of the near-surface air temperature along valley slopes is representative of the vertical profile of temperature in free atmosphere. Therefore, it was possible to solve a statistical regression with Eq. (8), computing the best fit parameters using the DTM height as an input.

2.1.1.3. Air humidity. According to the Clausius-Clapeyron law, the water vapour content in air increases exponentially with temperature; since T_a decreases approximately linearly with altitude and H_a decreases with height with an exponential behaviour. Based on that, a linear regression was used to map H_a over the domain starting from the observed variables:

$$\log H_a = c_0 + c_1 z \tag{9}$$

Once the absolute humidity was reconstructed for the domain, it was possible to compute the saturation and actual vapour pressures (Foken and Nappo, 2008).

2.1.1.4. Dew deposition and ground heat flux. In mountainous areas, nocturnal dew deposition can make a remarkable contribution to the water budget (Jacobs et al., 2006). Either evapotranspiration or dew formation can be estimated with the following equation (Garratt, 1992; Jacobs et al.,2006):

$$LE = \lambda ET = \frac{s}{s+\gamma}(R_n - G) + \frac{\gamma}{s+\gamma}\frac{\rho_{air}\lambda(q_s - q_a)}{r_a} \tag{10}$$

The proposed model also includes a routine for the hourly ($\Delta t = 1h$) dew estimation, according to the following relationships:

$$D = LE\,\Delta t \quad \text{if } LE \leq 0 \tag{11}$$

$$D = 0 \quad \text{if } LE > 0$$

The ground heat flux can be estimated as a fraction of net radiation R_n (Moran et al., 1994). Assuming an homogeneous 30-cm height vegetation cover on the entire domain, G can be estimated with a good approximation (as also verified by the measured data) as.

$$G = 0.05 R_n \tag{12}$$

2.1.1.5. Wind, precipitation and atmospheric pressure. Given that wind and rainfall fields are characterized by significant spatial and temporal intermittence, especially in mountain areas (Rebora et al., 2006), in the CLIME-MG model a constant value of wind speed for the entire domain was used (i.e. by averaging the measured hourly data of AWS). This approach was adopted given that it is impossible to realistically estimate the temporal and spatial variability of the wind using datasets from just a few AWS. For precipitation, each point, identified by a Voronoi partitioning of the domain, was assigned the rainfall amount measured at the nearest station.

Pressure was computed according to the hydrostatic equilibrium law. The air density was assumed constant throughout the domain, also because pressure values do not play a major role in evapotranspiration estimates.

2.1.2. Soil-water balance (SWB) module

As climatology is heavily affected by topography in mountain areas (Fridley, 2009), a high-resolution DTM is the main input for the model.

In addition, given that evapotranspiration is mainly a vertical 1D process along the shallower soil's horizons, a simple bucket soil model is here presented for the water-balance evaluation.

2.1.2.1. Soil depth. Soil depth information is often missing. In this work it is estimated with a process-based approach built on the local high-resolution topography (provided by the DTM) and some empirical parameters (Dietrich et al., 1995). This model assumes a net sediment transport vector, q_{soil}, downslope of soil converted from bedrock by biogenic and climate processes at a rate proportional to the gradient (i.e. $q_{soil} = -K\nabla z$). The mass conservation equation can be written as the balance between the local rate of bedrock-soil production, $f(z_s)$, and the divergence of the transport vector:

$$K\nabla^2 z = \frac{\delta z_s}{\delta t} - \frac{\rho_{rock}}{\rho_{soil}} f(z_s) \tag{13}$$

In the model, $f(z_s)$ is assumed to decrease exponentially. This hypothesis was suggested in previous studies (Dietrich et al., 1995; Heimsath et al., 1999):

$$f(z_s) = P_0 e^{-m/z_s} \tag{14}$$

Values of the empirical parameters for the implementation of the soil-depth model in Eq. (13) were chosen from literature and theoretical considerations. For our purposes, as described in Dietrich et al. (1995), the mean value of $K = 50 cm^2/yr$ was adopted, and ρ_r/ρ_s was set to 1.7. Pixels with exposed bedrock ($z_s = 0$, following the land-cover map) were included in order to estimate P_0. A lower limit for P_0 was also estimated; while m was determined by fitting $f(z_s)$ between $f(0) = P_0$ and $f(100) = 0.01 P_0$.

According to the aforementioned explanations, values of $P_0 = 0.009 cmyr^{-1}$, and $m = 0.045 cm^{-1}$ were computed. Measured soil depths in Gimillan (by means of electrical resistivity tomography - Raffelli et al., 2017) and in Valnontey (by simple vertical insertion of steel rods) - Aosta, Italy -, when compared with modelled values gave a robust agreement. The same method by Dietrich was used with the same scopes by Bertoldi et al. (2006), using the model GEOtop.

2.1.2.2. Soil-water balance. An original soil model was designed for describing soil moisture evolution over time. Following Ritchie (1998), the soil vertical profile z_s of each pixel was partitioned in several communicating layers with incremental thickness, starting from 50 mm the shallowest, followed by, respectively, two 100 mm, one 300 mm, and three deeper layers 500 mm thick (Fig. 2).

According with observations, all the inputs (i.e. water) entered into the system from the soil surface with higher variability in the superficial layers, and smoother behaviour at depth. The external positive inputs considered were precipitation and dew. The *AET* was the negative term of the balance and affected the first non-empty layer from the surface. Each layer was approximated as a bucket for which the Total Available Water (TAW) was considered the maximum amount of storable water, computed as:

$$TAW = \rho_s z_l \tag{15}$$

where ρ_s was set to 0.2, and the values 0.3 and 0.4 were used in the sensitivity analysis.

Percolation (*Perc*) occurred when the maximum storable capacity was achieved and, therefore, the exceeding water moved outside the layer. Water percolation from the deepest layer, being not relevant for the *AET* computation, was assumed lost by the system. The water-balance was computed in each layer (l) as a sum of positive and negative fluxes (Allen et al., 1998) considering the water availability, $0 \leq W_l \leq TAW$:

$$W_l(t) = W_l(t-1) + P(t) + D(t) - AET(t) - Perc(t) \quad l = 1 \tag{16}$$
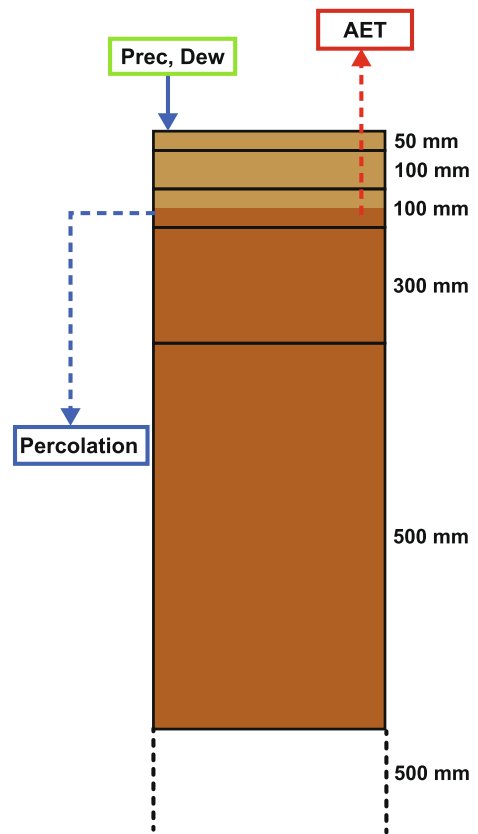
Fig. 2. Soil model scheme. Each layer is represented as a bucket of increasing thickness with depth. Precipitation enters from the surface and moves downward when each preceding layer is full. *AET* works inversely emitting water first from the surface then deeper layers as the shallower ones become empty.

$$W_l(t) = W_l(t-1) + Perc(t, l-1) - Perc(t, l) - AET(t) \quad l = 2 \cdots .n$$

As shown by Tromp-Van Meerveld and McDonnell (2006), at the end of the snow-melt season (i.e., April or May in the Alps), the soil water content is not affected by topography and it is approximately constant along the vertical soil profile with initial values corresponding to $W_l(t = 0) = 0.7 TAW$.

The model computes *AET* by using Eq. (17) (Allen et al., 1998):

$$AET = K_s K_c PET \tag{17}$$

Lookup tables with estimated vegetation coefficient already exist especially for crops and pastures (Allen et al., 1998). For the purposes of this work, alpine grasslands were here considered as extensive pastures with value of $K_c = 0.7$.

K_s was estimated for each soil layer according to Allen et al. (1998). For the sake of completeness, however, several other linear and non-linear models (e.g concave and convex) are available in literature (e.g. Raes et al., 2009) for any specific need. The root zone depletion (i.e. depletion fraction) for extensive pastures was also adopted. The model computes the stress coefficient for each pixel with a weighted average of the K_s coefficient associated with each layer:

$$K_s = \sum_{i}^{n} \frac{K_{s_i}}{w_i} n \quad \text{where} \quad w_i = \frac{z_{l_i}}{\sum z_l} \tag{18}$$

In the model, the area defined as grasslands was derived using the land cover map and was assumed to have homogeneous and full-covered grass. The presence of bare soil in the investigated mountain grassland surfaces being negligible, evaporation from bare soil was not included in the *AET* computation.

2.2. Study site and datasets

The studied area (Fig. 3) is situated in North-western Italy in the Aosta Valley (AO) Region (45. 462 N − 45.670 N; 7.145 E − 7.518 E) and it covers about 600 km^2. Grasslands here are located in a range between 1500 m and 3300 m a.s.l. The highest alpine peak of the area is the Gran Paradiso mountain: 4061 m a.s.l., and the spatial domain presents a very complex morphology.

Being sufficient to describe the aspect and the shading, a 10 m resolution DTM was aggregated at 30 m. To this end, the existing DTM has been resampled from 10 to 30 m using a nearest neighbour interpolation. This resolution was selected also to superimpose the Landsat satellite images, needed for the spatial validation. The land cover map "Carta della Natura" (Angelini et al., 2009), provided by ARPA VdA, with a spatial resolution of 30 m, was also used to select grassland areas in the domain.

Meteorological data were retrieved from 12 AWS located in the considered domain and managed by the *Aosta Valley "Regional Functional Center"* and the *Aosta Valley "Regional Environmental Protection Agency"* (ARPA VdA). Data were provided with 30 min time-step, then aggregated at 1 h. The available meteorological variables of each station are shown in Table 1.

The studied period lasted from June 1st to August 31st for the years 2014 and 2015.

2.3. Temporal and spatial validation of AET

2.3.1. Temporal validation of AET using eddy covariance

For the temporal validation of *AET*, data from two research measurement stations located in high mountain areas were used. One station was placed in Gimillan (Cogne, Aosta Valley, Italy) at 1730 m a.s.l. on a 26° slope facing S-SE (at the coordinates 45°36′ N and 7°21′ E). The other station was installed near the Nivolet Pass (Valsavarenche, Aosta Valley, Italy) on an almost flat small plateau of a steep ridge (about 32°) with a S-SE aspect at an altitude of 2555 m a.s.l. (Latitude: 45°52′ N; 7°17′ E). Collected data allowed the *AET* estimation by using the eddy

covariance technique. Night-time ET data and lower than zero ET values were assumed to be zero. Initialization periods and unrobust gap filled periods were excluded.

Both the two sites were equipped with a sonic anemometer (CSAT3, Campbell Scientific) and an open-path infrared gas analyser (LI-7500A, LI-COR), with which both sensible and latent heat fluxes were measured adopting the eddy-covariance technique - using the EddyPro SW (developed by LI-COR). Radiation and soil moisture were measured using, respectively, a four components radiometer (NR01, Hukseflux) and water content reflectometers (CS616, Campbell Scientific).

The first site has shrubs and grass, while the second is mainly a grassland.

2.3.2. Spatial validation of AET using METRIC

METRIC (Mapping EvapoTranspiration at high Resolution with Internalized Calibration) is a well-known model proposed by Allen et al. (2007). It maps *AET* by means of satellite-based data and image processing and it is based on the radiative energy balance closure assumption (considering the storage term negligible). Through the model it is possible to obtain an instantaneous *AET* value when the satellite passes over the domain.

The following inputs were used for the METRIC model:

- available Landsat 8 images in the visible and infrared spectral regions;
- a digital elevation model;
- a weather station measuring vapour pressure and wind speed.

The retrieved Landsat 8 satellite images have a pixel size of 30 m. The satellite passes every 16 days, but image quality and availability depend on weather conditions, thus for the time period studied, only 3 acquisitions were available: 27 August 2014, 13 July 2015, and 30 August 2015. The fly-over time was almost constant at about 10:15 UTC. Satellite images were used to calculate the Top of Atmosphere (TOA) reflectance. The conversion from digital numbers to TOA reflectance was computed according to USGS (2019). The other inputs used in
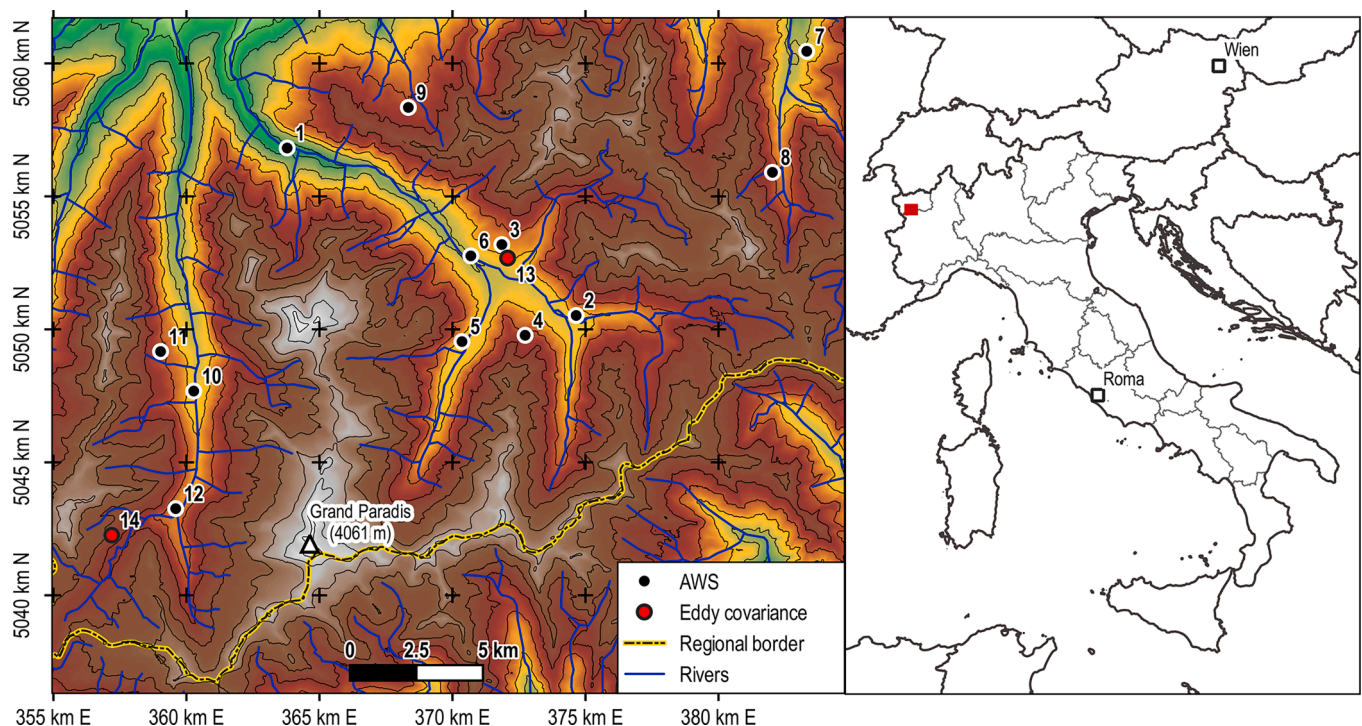

Fig. 3. Automatic Weather Stations (AWS, 1–12) and eddy covariance stations (13,14) location within the DTM domain.

Table 2
Meteorological and soil moisture data recorded at the Eddy Covariance monitoring station in Gimillan during the three selected days (i.e. satellite passages in good weather conditions).

Date	Air Temperature [°C]			R_n Avg (Whole day) $[W/m^2]$	R_n Avg (Daytime only) $[W/m^2]$	RH Avg [%]	Vol. soil moisture [-]
	Min	*Max*	*Avg*				
27/08/2014	6.5	20.1	12.4	179.8	389.1	53.7	0.11
13/07/2015	11.4	25.5	18.1	187.1	344.3	39.5	0.04
30/08/2015	9.9	22.9	15.7	188.2	409.0	64.6	0.12

METRIC were: the digital elevation model of Aosta valley (same DTM used for the CLIME-MG model), and the vapour pressure / wind speed data measured in Cogne meteorological station. A synoptic chart of the environmental conditions which occurred at the three satellite passes is represented in Table 2. Data identify ideal meteorological conditions with good weather situations and two different soil moisture levels (including a very dry date).

To compute the daily cumulative *AET* value from instantaneous METRIC data, the equation (55) in Allen et al. (2007) was adopted.

Some advantages and limits of METRIC can be summarized as follows.

i) METRIC was originally developed for flat and gently sloping large areas. This fact leads to some changes for the computation of variables affected by orography, such as the incident solar radiation. In particular, the incoming solar radiation computation adopted in METRIC (i.e. Eq. (19)), gives the total amount of solar radiation (i.e. direct and diffuse), without considering shading effects:

$$SW_{in} = \frac{G_{sc}\cos(\theta_{rel})\tau_{sw}}{d^2} \quad (19)$$

ii) A relevant source of uncertainty of METRIC outputs is the sensible heat component because of the internal calibration procedure. The sensible heat is computed as follows:

$$H = \rho_{air}c_p\Delta T/r_a \quad (20)$$

In this equation the term ΔT is computed with an internal calibration

and it is necessary to choose a "hot" and a "cold" pixel, for which the sensible heat fluxes are known (or easily computable).

For this work, the "cold" pixel was set over an alpine lake located within the domain, hence *AET* is equal to *PET* which was computed using the Priestley-Taylor equation (using the METRIC provided variables). The "hot" pixel was set where *H* was supposed to be maximized, such as a pixel with shallow soil depth, facing S-E, with scarce vegetation and high temperature (namely the steep pasture of Gimillan site used for the eddy covariance monitoring where *H* was measured).

3. Results and discussion

3.1. Model temporal validation

The soil–water balance (SWB) module is validated on a daily basis by comparing model outputs (i.e. *AET* and soil water content values) with observed data measured at the two Eddy Covariance stations located in two grassland sites (i.e. Gimillan and Nivolet).

In Fig. 4, the daily time series of measured and modelled *AET* are displayed together with the rainfall events (depicted in grey colour). A comparison is presented between the performance of the soil model alone (therefore using the local meteorology but without the meteorological spatial interpolation, abbreviated with "wmi" in the legend), and the performance of the complete meteorological and soil model (without using the AWS within a radius of 10 km from each eddy covariance measurement site). The performance of the SWB-module appears quite
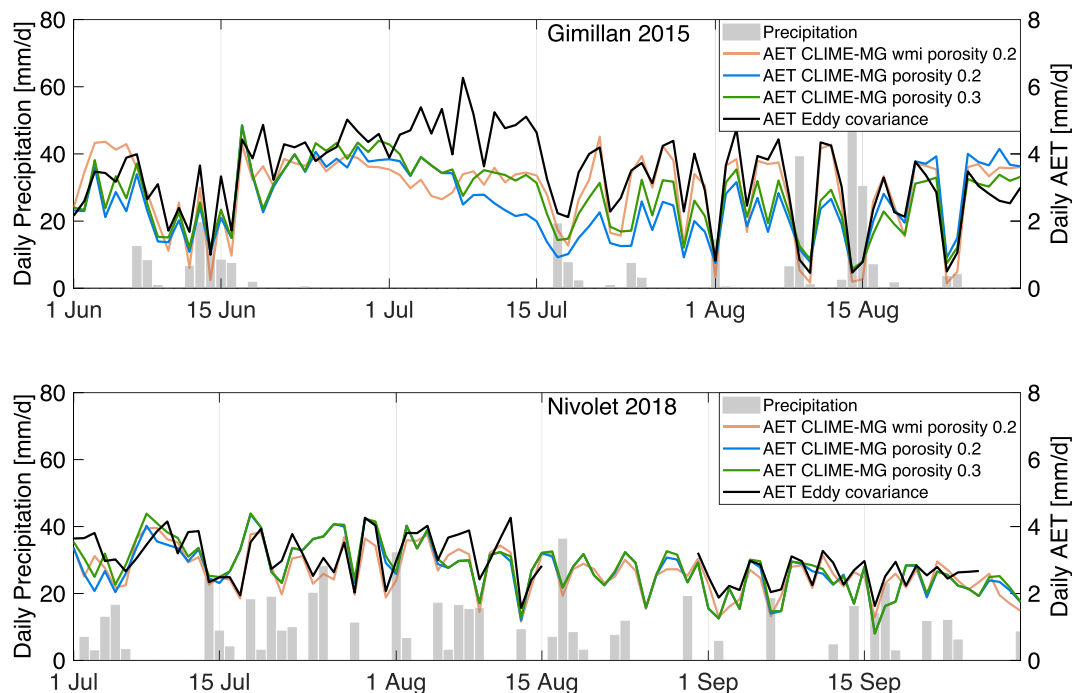
Fig. 4. Daily *AET* time series comparison between data measured by eddy covariance stations at Gimillan and Nivolet (black lines) and values modelled with CLIME-MG model with different soil porosity values (coloured lines); the term "wmi" identifies a model simulation without meteorological interpolation. Daily precipitation data are also shown in grey.
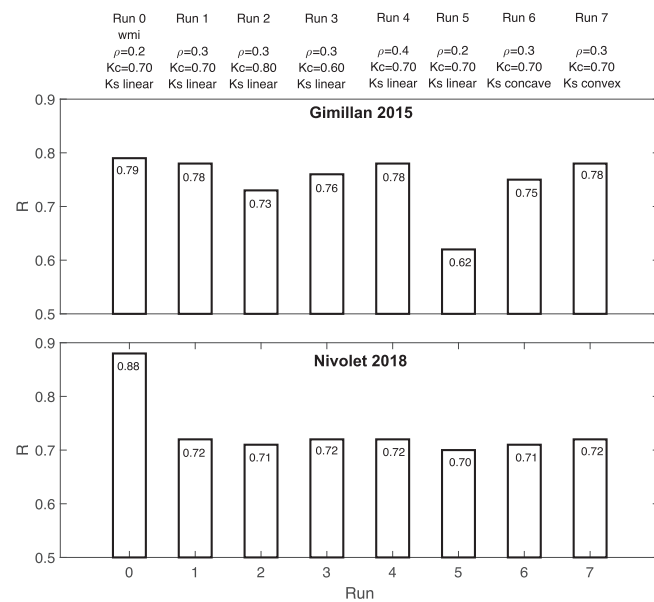
Fig. 5. Sensitivity of the coefficient of correlation between measured and modelled evapotranspiration in response to: (Run 0) absence of meteorological interpolation ("wmi", without meteorological interpolation); (Runs 1, 2 and 3) variation of crop coefficient Kc; (Runs 4 and 5) variation of effective porosity ρ; (Runs 6 and 7) variation of vegetation stress coefficient Ks, respectively for the Gimillan 2015 and Nivolet 2018 cases.

good in both cases and the correlation is quantified in Fig. 5. The agreement with eddy covariance data was found especially in wetter periods with recurring rainfall events. On the other hand, during the long dry period at the end of July 2015, measured and modelled data remain quite separated, with an evident underestimation of the modelled data. This behaviour can be partially due to the encroachment of shrubs into this abandoned pasture with deeper uptake capacities of water (e.g. Gisolo et al., 2022; van den Bergh et al., 2018). Similar behaviour was also highlighted by Wegehenkel and Beyrich (2014) in a grass-covered field site located in north-eastern Germany, and by Ochoa-Sánchez et al. (2019) in high Andean grasslands where the adopted hydrological model (i.e. PDM model - Moore and Clarke, 1981) demonstrated good performance of *AET* quantification but with evident underestimations in water scarce conditions. Contrarily, Rigon et al. (2006), using the GEOtop model, pointed-out in the Little Washita watershed (Oklahoma), an overestimation of *AET* in summer conditions (with respect to the measured values) since the presence of bare soil in mixed vegetation pixels (e.g. agricultural processes) can significantly alter the average fractional vegetation cover.

A model sensitivity test was conducted to verify the output variability versus some aspects considered to play a major role in the modelling process. In particular, the adoption (or not) of the meteorological interpolation, as well as three parameters affecting the soil–vegetation atmosphere relationship (namely the effective soil porosity – ρ; the vegetation coefficient – K_c; and the vegetation stress coefficient – K_s) were investigated. For this purpose, several model runs were performed at both the Gimillan and Nivolet experimental sites based on the following settings: 1) fixing of soil-vegetation parameters ($\rho = 0.2$; $K_c = 0.7$; K_s estimated with a linear model) but variation of the meteorological interpolation (presence - absence); 2) fixing of the meteorological interpolation but variation, one by one, of the soil-vegetation parameters (ρ values = 0.2, 0.3 and 0.4; K_c values = 0.60, 0.70 and 0.80; and K_s estimated with three models, namely linear, convex and concave). The sensitivity analysis was performed by computing the coefficient of correlation between modelled and observed evapotranspiration data.

Based on the results (Fig. 5), runs without meteorological interpolation were characterized by higher performances, especially at the Nivolet site, where vegetation is pure grassland (without presence of shrubs like at Gimillan). On the contrary, runs with meteorological interpolation show better results for the Gimillan site. This can be due to the elevation of the Nivolet site, which is much higher than all the AWS used for the interpolation (and the orographic correction may introduce further degrees of uncertainty).

Results of Fig. 5 also highlight that the changing of the three soil-vegetation parameters has limited effect at both sites. As a general consideration, Clime-MG showed better performance/reliability in non-limiting conditions of water availability (as demonstrated by results obtained in the growing season without long dry periods). Vice versa, it is interesting to point-out the Gimillan run with $\rho = 0.2$, $K_c = 0.70$, and K_s = linear, showing a low coefficient of correlation (R = 0.62). This specific weak performance (also compared with the same run at the Nivolet site carried-out with the same set of parameters) might be explained by the dry period that occurred in July 2015, characterized by high air temperature and low relative humidity (Fig. 1), and, hence, by a water scarcity (as illustrated also in Fig. 6).

In Fig. 6, the daily soil moisture at the Gimillan monitoring site is presented, comparing the CLIME-MG model outputs and the measured *AET* data for the same growing season 2015. The average measured values between 20 and 40 cm of soil depths are reported in comparison with the average modelled value between surface and 50 cm. The modelling results are shown both for the soil model alone and for the complete meteorological and soil model. This means that in the first case the meteorological inputs are taken at a single point, close to the eddy covariance site, without the meteorological interpolation part of the model (acronym "wmi"), while in the second case the meteorological part of the model (without using the AWS in a radius of 10 km from each eddy covariance measurement site). Also, there is a comparison between porosity equal to 0.2 and to 0.3. The effect of the drought between 1st and 15th July is evident in all graphs, consistent with the *AET* modelling results.

3.2. Spatial validation of the model

3.2.1. Analysis and insights across the whole domain

In this section, CLIME-MG outputs are compared to METRIC ones (obtained from satellite images analysis) to evaluate the performances of the CLIME-MG model over the whole geographical domain. In Fig. 7, the results for the 30 August 2015 satellite acquisition at the hourly time scale (acquisition time: about 10 AM CET), are shown. The difference in
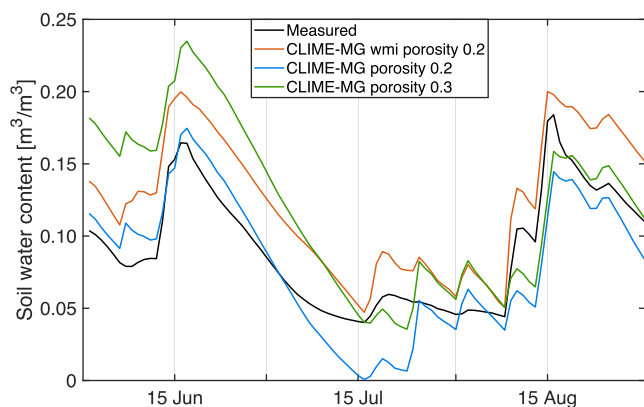
Fig. 6. Comparison of daily soil moisture measured at Gimillan in the year 2015 with the modelled values. The black line represents the average of data from 20 cm and 40 cm depths measured daily; the coloured lines represent the average modelled soil moisture between the surface and 50 cm depth, obtained from CLIME-MG (using different soil porosity values); the term "wmi" identifies a model simulation without meteorological interpolation.

values, both with respect to the average values computed with METRIC across the whole domain, is depicted.

In both CLIME-MG and METRIC, those differences have a similar spatial structure controlled by the DTM (leading also to a general agreement of the two models in both the maximum and minimum *AET* localised zones). In these complex morphologies, CLIME-MG seems to depict more restrained dynamics than METRIC which, instead, shows a general tendency to settle on more extreme values. CLIME-MG usually highlights lower *AET* values than METRIC. Despite the noticeable local specific variability, these characteristics were observed on all the three available dates. These plots are to be analysed jointly with the plot in Fig. 8, where the differences between CLIME and METRIC are plotted against morphological characteristics, namely elevation, aspect, soil depth and slope. Elevation and slope show a trend in all the three available dates for both hourly and daily data, whilst aspect doesn't seem to highlight any trend. Soil depth shows a trend except for the 13th of July date, which corresponds to the drought already discussed in the temporal analysis. These trends suggest possible future improvements of

CLIME to capture more tightly the spatial variability of *AET*.

Statistical measures are reported in Table 3, using the SPAEF index (Koch et al., 2018) and NRMSE. Despite values seem to be lower with respect to traditional calibrated models, they can be considered satisfactory for a calibration free model, especially in wet conditions. In the driest date the value is much lower but this situation regards only few days during the two growing seasons studied. As a general observation, the hourly mean *AET* data showed higher values for METRIC than CLIME-MG.

*3.2.2. Comparison among selected areas*

To investigate a possible degradation of CLIME-MG modeling results as the distance from the sources of data input increases (i.e. proximity / remoteness of AWS (i.e. where meteorological input data were measured)), ten small square area subsamples (1.8 km × 1.8 km) were identified within the whole domain (Fig. 9). The selected squares were grouped in: i) areas within which an AWS was located, ii) areas where AWS were located in proximity, and iii) areas far from AWS. Modeling output on each subsample was used to compute statistical indexes to verify if and how results were affected by distance to the AWS.

In Fig. 10, the spatial correlation coefficient *R* and the normalized root mean square error (*NRMSE*) are shown. Values were computed using hourly evapotranspiration output of CLIME-MG and METRIC over the areas identified by the tiles in Fig. 9. The statistical measures show that outputs were not significantly affected by the proximity / remoteness of the AWS.

Since the weather stations are not uniformly distributed by elevation, as shown in Table 1, CLIME-MG consistency was also tested at altitudes where no measurement stations were available. The maximum elevation of the AWS network was below 2300 m, while the studied grasslands were located up to 3300 m. Fig. 11 shows statistical measures of this analysis. Even in this test, the absence of AWS at high elevations does not affect the CLIME-MG outputs. However, in the temporal analysis at the higher altitude Nivolet site, the correlation coefficients are lower than at Gimillan site.

4. Conclusions

Alpine regions, being usually characterized by complex terrains, limited accessibility, and a challenging measurement environment
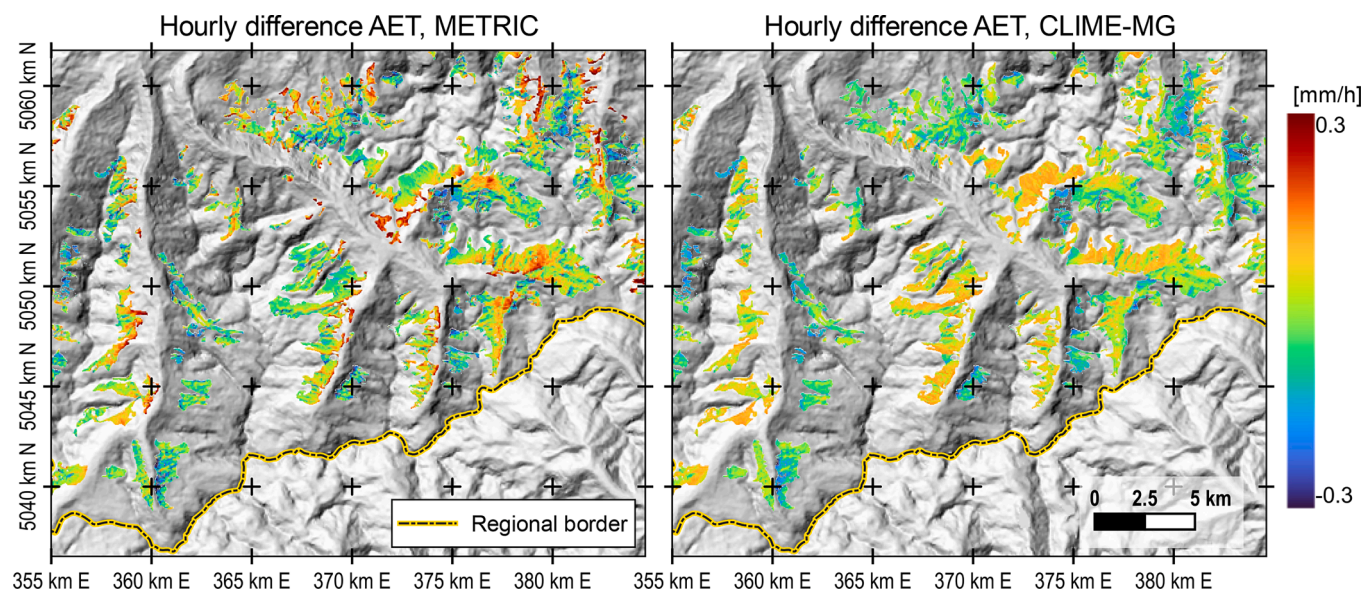
Fig. 7. Spatial variability of differences [*mm/h*] in hourly *AET* between – pixel by pixel - METRIC (left) and CLIME-MG (right) with respect to the overall domain *AET* average value –on Aug 30, 2015, at 10:15 am.
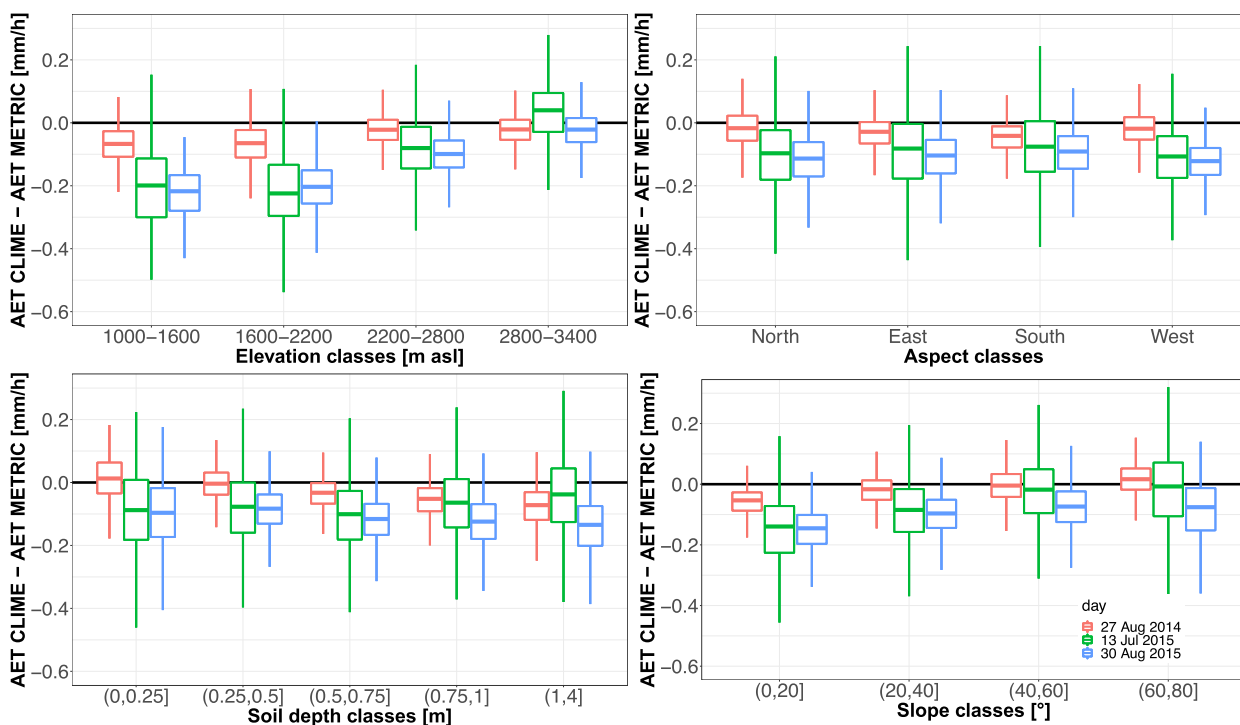
Fig. 8. Boxplots of the hourly differences between CLIME-MG and METRIC models' outputs versus elevation, aspect, soil depth and slope (during the three available dates: Aug.27, 2014; Jul.13, 2015; Aug.30, 2015).

Table 3

Comparison between METRIC and CLIME-MG models (hourly *AET*). SPAEF index (SPAtial EFficiency index, Koch et al., 2018); SPAEF index components (i.e coefficient of correlation; coefficients of variation ratio (CV_{METRIC}/CV_{CLIME}); histogram match), and normalized root mean square error (NRMSE) for all the available satellite passages.

	SPAEF	Correlation coefficient	CV ratio	Histogram match	NRMSE
27 August 2014	0.33	0.90	0.43	0.41	0.18
13 July 2015	0.21	0.49	0.60	0.55	0.44
30 August 2015	0.34	0.75	0.88	0.41	0.30

suffer from a limited quantity and quality of information as well as limited availability of modelling tools for characterizing actual conditions, and providing forecasts and simulations of future scenarios (especially at local scale). Starting from the observation that much of the spatial and temporal variability of *AET* in high altitude areas can be explained by aspect, shading, and slope in conjunction with land cover and meteorological solar radiation forcing (which are, respectively, spatially and temporally highly variable in mountains), the objective of this work was to present and validate a new calibration free soil water model (i.e. CLIME-MG) for computing the soil–water balance and mapping the actual evapotranspiration *(AET)* starting from easy-to-find inputs (i.e. digital terrain model (DTM), land cover map, and standard meteorological data retrieved from conventional weather stations). All the parameters of the model are fixed and taken from literature, without any calibration.

The proposed model consists of two main modules: the "meteorological module" which uses meteorological data to compute the potential evapotranspiration with the Penman-Monteith formula, and the "soil–water balance module" which computes the soil–water balance with an original model to estimate the vegetation stress coefficient, and thus *AET* and soil moisture.
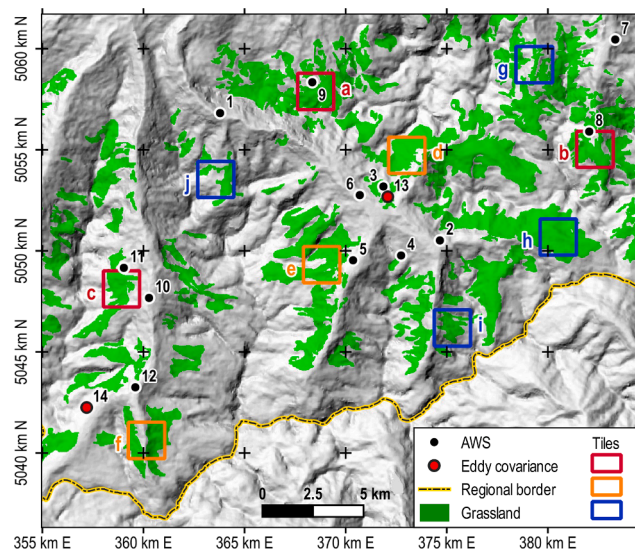

Fig. 9. Locations of the tiles where the effect of proximity to an AWS was analyzed. Red = areas within which an AWS is located; orange = areas were AWS are within 3 km; blue = areas far from AWS.

The model was validated using temporal and spatially distributed data. Temporal validation was performed with two time series of *AET* measured at eddy covariance stations located at Gimillan and Nivolet Pass (respectively at 1730 m and 2555 m a.s.l.; Aosta Valley, Italy). Spatial validation was performed by comparison with the Landsat-based METRIC model *AET* output.

Results show good temporal performance with daily data especially in wetter periods with recurring rainfall events. The performance of the model both with local meteorological data (to test the soil model only) and with the complete meteorological interpolation (without using the AWS within a radius of 10 km from each eddy covariance station) was
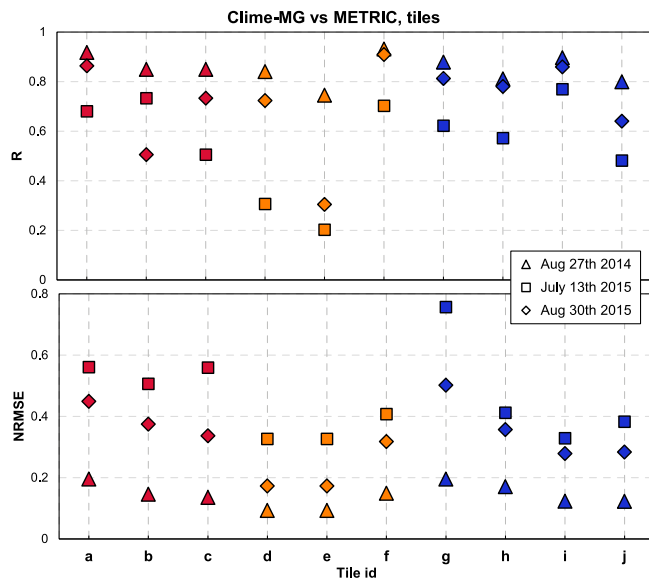
Fig. 10. Correlation coefficient *R* and *NRMSE* between the hourly evapotranspiration output of CLIME-MG and METRIC over the areas identified by the tiles of Fig. 9. Red color refers to areas within which an AWS is located (tiles from "a" to "c"); orange refers to areas were AWS are located in proximity (tiles from "d" to "f"); blue color refers to areas far from AWS (tiles from "g" to "j").
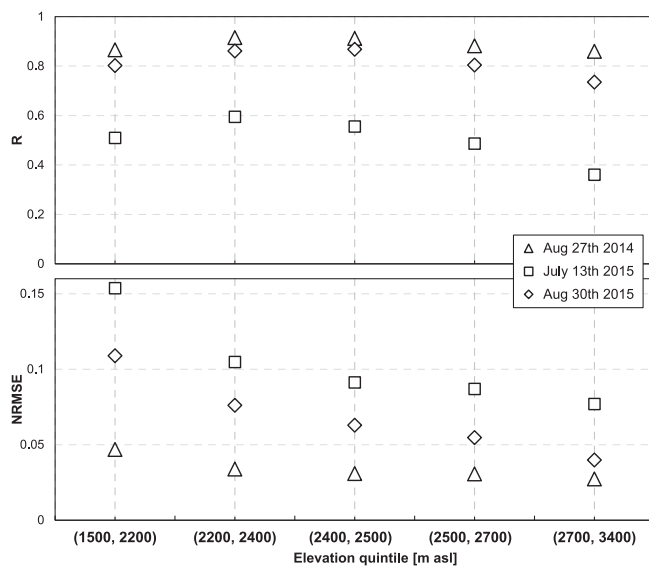
Fig. 11. Correlation coefficient (R) and *NRMSE* between CLIME-MG and METRIC computed for hourly actual evapotranspiration values, according to elevation ranges.

also investigated with good results. In addition, the correlation coefficient sensitivity to three key parameters of the soil model, namely the effective porosity, the cultural coefficient K_c and the stress coefficient K_s, was shown to be quite low.

The spatial validation confirms the high correlation between the outputs of the two models, CLIME-MG and METRIC, (with a similar spatial structure controlled by the DTM). Boxplots of deviations between CLIME and METRIC with respect to morphological characteristics has highlighted some dependency on elevation, slope and soil depth (but not on aspect); this confirms the great influence of topography on the grassland *AET* processes and suggests the possibility of future improvement of this simple model. Finally, spatial results demonstrated the non-sensitivity of the proposed model to local elevation and to the

distance from a meteorological station.

Concluding, CLIME-MG model proved to perform well for mountainous grassland *AET* modelling. Further applied studies will be essential to both confirm the robustness of the proposed approach and to adapt (including necessary adjustments of the literature parameters) the here proposed tool to different land covers types, here not investigated.

Author contributions

Balocco, Boetti, Dematteis, Ferraris: First conceptualization and software drafting. *Bevilacqua, Ferraris, Gisolo*: Conceptualization and model/methodology definition, Software implementation/verifications, and Output visualization. *Canone, Ferraris, Gisolo, Previati*: Investigation, Data acquisition and Data curation. *Bevilacqua, Gentile, Gisolo, Nsassila*: Data analysis. *Gisolo, Previati*: Writing- Original draft preparation and further reviews. *Ferraris, Heery, Vereecken*: Supervision, Writing- critical review and commentaries. *Ferraris, Previati*: Project administration and Funding acquisition/management.

Declaration of Competing Interest

The authors declare that they have no known competing financial interests or personal relationships that could have appeared to influence the work reported in this paper.

Conflicts of interest.

The authors declare no conflict of interest.

References

Aguilar, C., Herrero, J., Polo, M., 2010. Topographic effects on solar radiation distribution in mountainous watersheds and their influence on reference evapotranspiration estimates at watershed scale. Hydrol. Earth Syst. Sci. 14 (12), 2479–2494. https://doi.org/10.5194/hess-14-2479-2010.

Alexander, J., Diez, J., Levine, J., 2015. Novel competitors shape species' responses to climate change. Nature 525, 515–518. https://doi.org/10.1038/nature14952.

R.G. Allen L.S. Pereira D. Raes M. Smith Crop Evapotranspiration: Guidelines for Computing Crop Water Requirements, United Nations Food and Agriculture Organization, Irrigation and Drainage Paper 56 1998 Rome, Italy 300 pp. ISBN 92-5-104219-5.

Allen, R.G., Tasumi, M., Trezza, R., 2007. Satellite-Based Energy Balance for Mapping Evapotranspiration with Internalized Calibration (METRIC) – Model. J. Irrig. Drain. Eng. 133 (4), 380–394. https://doi.org/10.1061/(ASCE)0733-9437(2007)133:4 (380).

Angelini, P., Augello, R., Bagnaia, R., Bianco, P., Capogrossi, R., Cardillo, A., Ercole, S., Francescato, C., Giacanelli, V., Laureti, L., Lugeri, F., Lugeri, N., Novellino, E., Oriolo, G., Papallo, O., Serra, B., 2009. Il progetto Carta della Natura. Linee guida per la cartografia e la valutazione degli habitat alla scala 1:50.000. ISPRA, Rome, pp. 128. ISBN 978-88-448-0381-0.

Asse, D., Chuine, I., Vitasse, Y., Yoccoz, N.G., Delpierre, N., Badeau, V., Delestrade, A., Randin, C.F., 2018. Warmer winters reduce the advance of tree spring phenology induced by warmer springs in the Alps. Agric. For. Meteorol. 252, 220–230. https://doi.org/10.1016/j.agrformet.2018.01.030.

Auer, I., Böhm, R., Jurkovic, A., Lipa, W., Orlik, A., Potzmann, R., Schöner, W., Ungersböck, M., Matulla, C., Briffa, K., Jones, P., Efthymiadis, D., Brunetti, M., Nanni, T., Maugeri, M., Mercalli, L., Mestre, O., Moisselin, J.-M., Begert, M., Müller-Westermeier, G., Kveton, V., Bochnicek, O., Stastny, P., Lapin, M., Szalai, S., Szentimrey, T., Cegnar, T., Dolinar, M., Gajic-Capka, M., Zaninovic, K., Majstorovic, Z., Nieplova, E., 2007. HISTALP—historical instrumental climatological surface time series of the Greater Alpine Region. Int. J. Climatol. 27 (1), 17–46.

Bastiaanssen, W.G.M., Menenti, M., Feddes, R.A., Holtslag, A.A.M., 1998. A remote sensing surface energy balance algorithm for land (SEBAL), 1. Formulation. J. Hydrol. 212–213, 198–212. https://doi.org/10.1016/S0022-1694(98)00253-4.

Bastiaanssen, W., Noordman, E., Pelgrum, H., Davids, G., Thoreson, B., Allen, R., 2005. Sebal model with remotely sensed data to improve water-resources management under actual field conditions. J. Irrig. Drain. Eng. 131 (1), 85–93. https://doi.org/10.1061/(ASCE)0733-9437(2005)131:1(85).

Basu, N.B., Rao, P.S.C., Winzeler, H.E., Kumar, S., Owens, P., Merwade, V., 2010. Parsimonious modeling of hydrologic responses in engineered watersheds: structural heterogeneity versus functional homogeneity. Water Resour. Res. 46 (4), W04501. https://doi.org/10.1029/2009WR007803.

Baveye, P.C., Labac, M., 2015. Moving away from the geostatistical lamppost: Why, where, and how does the spatial heterogeneity of soils matter? Ecol. Model. 298, 24–38. https://doi.org/10.1016/j.ecolmodel.2014.03.018.

Beniston, M., Stoffel, M., 2014. Assessing the impacts of climatic change on mountain water resources. Sci. Total Environ. 493, 1129–1137. https://doi.org/10.1016/j.scitotenv.2013.11.122.

Bertoldi, G., Rigon, R., Over, T.M., 2006. Impact of Watershed Geomorphic Characteristics on the Energy and Water Budgets. J. Hydrometeorol. 7 (3), 389–403. https://doi.org/10.1175/JHM500.1.

Blaney, H.F., Criddle, W.D., 1950. Determining Water Requirements in Irrigated Areas from Climatological and Irrigation Data. USDA Soil Conserv. Serv. SCS-TP96, 48.

Bottazzi, M., Bancheri, M., Mobilia, M., Bertoldi, G., Longobardi, A., Rigon, R., 2021. Comparing Evapotranspiration Estimates from the GEOframe-Prospero Model with Penman-Monteith and Priestley-Taylor Approaches under Different Climate Conditions. Water 13, 1221. https://doi.org/10.3390/w13091221.

Bouma, J., 1989. Using soil survey data for quantitative land evaluation. In: Stewart, B.A. (Ed.), Advances in Soil Science, vol. 9. Springer Verlag, New York, pp. 177–213.

Brussolo, E., Palazzi, E., Von Hardenberg, J., Masetti, G., Vivaldo, G., Previati, M., Canone, D., Gisolo, D., Bevilacqua, I., Provenzale, A., Ferraris, S., 2022. Aquifer recharge in the Piedmont Alpine zone: Historical trends and future scenarios. Hydrol. Earth Syst. Sci. 26, 407–427. https://doi.org/10.5194/hess-26-407-2022.

W. Brutsaert Hydrology: an introduction 2005 Cambridge University Press 10.1017/CBO9780511808470 618.

Carter, C., Liang, S., 2018. Comprehensive evaluation of empirical algorithms for estimating land surface evapotranspiration. Agric. For. Meteorol. 256–257, 334–345. https://doi.org/10.1016/j.agrformet.2018.03.027.

Chen, H.S., Shao, M.A., Li, Y.Y., 2008. The characteristics of soil water cycle and water balance on steep grassland under natural and simulated rainfall conditions in the Loess Plateau of China. J. Hydrol. 360 (1–4), 242–251. https://doi.org/10.1016/j.jhydrol.2008.07.037.

Chirouze, J., Boulet, G., Jarlan, L., Fieuzal, R., Rodriguez, J.C., Ezzahar, J., Er-raki, S., Bigeard, G., Merlin, O., Garatuza-Payan, J., Watts, C., Chehbouni, G., 2013. Inter-comparison of four remote sensing based surface energy balance methods to retrieve surface evapotranspiration and water stress of irrigated fields in semi-arid climate. Hydrol. Earth Syst. Sci. Discuss. 10, 895–963. https://doi.org/10.5194/hessd-10-895-2013.

Chung, U., Yun, J.I., 2004. Solar irradiance-corrected spatial interpolation of hourly temperature in complex terrain. Agric. For. Meteorol. 126 (1), 129–139. https://doi.org/10.1016/j.agrformet.2004.06.006.

Cleugh, H.A., Leuning, R., Mu, Q., Running, S.W., 2007. Regional evaporation estimates from flux tower and MODIS satellite data. Remote Sens. Environ. 106, 285–304. https://doi.org/10.1016/j.rse.2006.07.007.

De la Fuente-Sáiz, D., Ortega-Farías, S., Fonseca, D., Ortega-Salazar, S., Kilic, A., Allen, R., 2017. Calibration of METRIC model to estimate energy balance over a drip-irrigated apple orchard. Remote Sens. 9 (7), 670. https://doi.org/10.3390/rs9070670.

Delpla, I., Jung, A.V., Baures, E., Clement, M., Thomas, O., 2009. Impacts of climate change on surface water quality in relation to drinking water production. Environ. Int. 35, 1225–1233. https://doi.org/10.1016/j.envint.2009.07.001.

Dietrich, W.E., Reiss, R., Hsu, M.L., Montgomery, D.R., 1995. A process-based model for colluvial soil depth and shallow landsliding using digital elevation data. Hydrol. Process. 9 (3–4), 383–400. https://doi.org/10.1002/hyp.3360090311.

Doorenbos, J., Pruitt, W.O., 1977. Crop Water Requirements. FAO Irrigation and Drainage Paper 24, Land and Water Development Division, FAO, Rome, pp.144.

Duguay, C.R., 1995. An approach to the estimation of surface net radiation in mountain areas using remote sensing and digital terrain data. Theor. Appl. Climatol. 52, 55–68. https://doi.org/10.1007/BF00865507.

Einhorn, B., Eckert, N., Chaix, C., Ravanel, L., Deline, P., Gardent, M., Boudières, V., Richard, D., Vengeon, J.-M., Giraud, G., Schoeneich, P., 2015. Climate change and natural hazards in the Alps. Observed and potential impacts on physical and socio-economic systems. J. Alpine Res. |. Rev. Geogr. Alp, 103–1102. https://doi.org/10.4000/rga.2878.

Evett, S.R., Schwartz, R.C., Howell, T.A., Baumhardt, R.L., Copeland, K.S., 2012. Can weighing lysimeter et represent surrounding field et well enough to test flux station measurements of daily and sub-daily ET? Adv. Water Resour. 50, 79–90. https://doi.org/10.1016/j.advwatres.2012.07.023.

Filippa, G., Cremonese, E., Galvagno, M., Bayle, A., Choler, P., Bassignana, M., Piccot, A., Poggio, L., Oddi, L., Gascoin, S., Costafreda-Aumedes, S., Argenti, G., Dibari, C., 2022. On the distribution and productivity of mountain grasslands in the Gran Paradiso National Park, NW Italy: A remote sensing approach. Int. J. Appl. Earth Obs. Geoinf. 108, 102718 https://doi.org/10.1016/j.jag.2022.102718.

Fisher, J.B., Melton, F., Middleton, E., Hain, C., Anderson, M., Allen, R., McCabe, M.F., Hook, S., Baldocchi, D., Townsend, P.A., Kilic, A., Tu, K., Miralles, D.D., Perret, J., Lagouarde, J.-P., Waliser, D., Purdy, A.J., French, A., Schimel, D., Famiglietti, J.S., Stephens, G., Wood, E.F., 2017. The future of evapotranspiration: Global requirements for ecosystem functioning, carbon and climate feedbacks, agricultural management, and water resources. Water Resour. Res. 53 (4), 2618–2626.

T. Foken C.J. Nappo Micrometeorology. Springer Science & Media 2008 10.1007/978-3-540-74666-9 308.

Fridley, J.D., 2009. Downscaling climate over complex terrain: high finescale ($<$ 1000 m) spatial variation of near-ground temperatures in a montane forested landscape (Great Smoky Mountains). J. Appl. Meteorol. Clim. 48 (5), 1033–1049. https://doi.org/10.1175/2008JAMC2084.1.

Fuhrer, J., Smith, P., Gobiet, A., 2014. Implications of climate change scenarios for agriculture in alpine regions - a case study in the Swiss Rhone catchment. Sci. Total Environ. 493, 1232–1241. https://doi.org/10.1016/j.scitotenv.2013.06.038.

Gallo, K., Hale, R., Yu, Y., 2011. Evaluation of the relationship between air temperature and land surface temperature under clear and cloudy sky conditions. J. Appl. Meteorol. Clim. 50 (3), 767–775. https://doi.org/10.1175/2010JAMC2460.1.

Garratt, J., 1992. The atmospheric boundary layer. Cambridge atmospheric and space science series, University Press, Cambridge, p. 316.

Gaudard, L., Romerio, F., Dalla Valle, F., Gorret, R., Maran, S., Ravazzani, G., Stoffel, M., Volonterio, M., 2014. Climate change impacts on hydropower in the Swiss and Italian Alps. Sci. Total Environ. 493, 1211–1221.

Gilaberte-Búrdalo, M., López-Martín, F., Pino-Otín, M.R., López-Moreno, J.I., 2014. Impacts of climate change on ski industry. Environ. Sci. Policy 44, 51–61. https://doi.org/10.1016/j.envsci.2014.07.003.

Gisolo, D., Bevilacqua, I., van Ramshorst, J., Knohl, A., Siebicke, L., Previati, M., Canone, D., Ferraris, S., 2022. Evapotranspiration in an abandoned grassland in the Italian Alps: influence of local topography, inter and intra-annual variability and environmental drivers. Submitted.

Gobiet, A., Kotlarski, S., Beniston, M., Heinrich, G., Rajczak, J., Stoffel, M., 2014. 21st century climate change in the European Alps - a review. Sci. Tot. Environ. 493, 1138–1151. https://doi.org/10.1016/j.scitotenv.2013.07.050.

Granier, A., 1987. Evaluation of transpiration in a Douglas-fir stand by means of sap flow measurements. Tree Physiol. 3 (4), 309–320. https://doi.org/10.1093/treephys/3.4.309.

Gu, S., Tang, Y., Cui, X., Du, M., Zhao, L., Li, Y., Xu, S., Zhou, H., Kato, T., Qi, P., Zhao, X., 2008. Characterizing evapotranspiration over a meadow ecosystem on the Qinghai-Tibetan Plateau. J. Geophys. Res. – Atmos. 113 (D8) https://doi.org/10.1029/2007JD009173.

Gürtz, J., Lang, H., Verbunt, M., Zappa, M., 2005. The use of hydrological models for the simulation of climate change impacts on mountain hydrology. In Global change and mountain regions, editors: Huber U.M., Bugmann H.K.M. and Reasoned M.A., Springer, pp. 343-354.

Haeberli, W., Beniston, M., 1998. Climate change and its impacts on glaciers and permafrost in the Alps. Ambio 27 (4), 258–265.

Hargreaves, G.H., Samani, Z.A., 1982. Estimating potential evapotranspiration. J. Irrig. Drain. Eng. 108 (3), 223–230.

Harris, C., Muhll, D., Isaksen, K., Haeberli, W., Sollid, J., King, L., Holmlund, P., Dramis, F., Guglielmin, M., Palacios, D., 2003. Warming permafrost in European mountains. Global Planet. Change 39, 215–225. https://doi.org/10.1016/j.gloplacha.2003.04.001.

Heimsath, A.M., Dietrich, W.E., Nishiizumi, K., Finkel, R.C., 1999. Cosmogenic nuclides, topography and the spatial variation of soil depth. Geomorphology 27 (1), 151–172. https://doi.org/10.1016/S0169-555X(98)00095-6.

Heinrich, G., Gobiet, A., Truhetz, H., Mendlik, T., 2013b. Expected climate change and its uncertainty in the Alpine region; extended uncertainty assessment of the reclip: century and ENSEMBLES multi-model dataset. Scientific Report 50. Wegener Center for Climate and Global Change, University of Graz, Austria.

Hemakumara, H.M., Chandrapala, L., Arnold, M.F., 2003. Evapotranspiration fluxes over mixed vegetation areas measured from large aperture scintillometer. Agric. Water Manage. 58 (2), 109–122. https://doi.org/10.1016/S0378-3774(02)00131-2.

Iqbal, M., 1983. An introduction to solar radiation. Academic Press, Toronto, p. 390.

Jacobs, A.F., Heusinkveld, B.G., Wichink Kruit, R.J., Berkowicz, S.M., 2006. Contribution of dew to the water budget of a grassland area in the Netherlands. Water Resour. Res. 42 (3), W03415. https://doi.org/10.1029/2005WR004055.

Jin, M.S., Mullens, T., 2014. A study of the relations between soil moisture, soil temperatures and surface temperatures using arm observations and offline clm4 simulations. Climate 2 (4), 279–295. https://doi.org/10.3390/cli2040279.

Jury, W.A., 1982. Simulation of solute transport using a transfer function model. Water Resour. Res. 18 (2), 363–368. https://doi.org/10.1029/WR018i002p00363.

Klanderud, K., Totland, O., 2005. Simulated climate change altered dominance hierarchies and diversity of an alpine biodiversity hotspot. Ecology 86, 2047–2054. https://doi.org/10.1890/04-1563.

Koch, J., Cüneyd Demirel, M., Stisen, S., 2018. The SPAtial Efficiency metric (SPAEF): multiple-component evaluation of spatial patterns for optimization of hydrological models. Geosci. Model Dev. 11, 1873–1886. https://doi.org/10.5194/gmd-11-1873-2018.

Kollet, S.J., Maxwell, R.M., 2006. Integrated surface-groundwater flow modeling: A free-surface overland flow boundary condition in a parallel groundwater flow model. Adv. Water Resour. 29 (7), 945–958. https://doi.org/10.1016/j.advwatres.2005.08.006.

Kumar, L., Skidmore, A.K., Knowles, E., 1997. Modelling topographic variation in solar radiation in a GIS environment. Int. J. Geogr. Inf. Sci. 11, 475–497. https://doi.org/10.1080/136588197242266.

Li, Z.L., Tang, R.L., Wan, Z.M., Bi, Y.Y., Zhou, C.H., Tang, B.H., Yan, G.J., Zhang, X.Y., 2009. A review of current methodologies for regional evapotranspiration estimation from remotely sensed data. Sensors 9 (5), 3801–3853. https://doi.org/10.3390/s90503801.

Malek, E., Bingham, G.E., 1993. Comparison of the Bowen ratio–energy balance and the water balance methods for the measurement of evapotranspiration. J. Hydrol. 146 (1–4), 209–220. https://doi.org/10.1016/0022-1694(93)90276-F.

Makkink, G.F., 1957. Testing the Penman Formula by Means of Lysimeters. J. Inst. of Water Eng. 11, 277–288.

Maran, S., Volonterio, M., Gaudard, L., 2014. Climate change impacts on hydropower in an alpine catchment. Environ. Sci. Pol. 43, 15–25. https://doi.org/10.1016/j.envsci.2013.12.001.

Massaro, G., Stiperski, I., Pospichal, B., Rotach, M.W., 2015. Accuracy of retrieving temperature and humidity profiles by ground-based microwave radiometry in truly complex terrain. Atmos. Meas. Tech. 8 (8), 3355–3367. https://doi.org/10.5194/amt-8-3355-2015.

Mastrotheodoros, T., Pappas, C., Molnar, P., Burlando, P., Manoli, G., Parajka, J., Rigon, R., Szeles, B., Bottazzi, M., Hadjidoukas, P., Fatichi, S., 2020. More green and less blue water in the Alps during warmer summers. Nat. Clim. Chang. 10, 155–161. https://doi.org/10.1038/s41558-019-0676-5.

McDonnell, J.J., Sivapalan, M., Vache, K., Dunn, S., Grant, G., Haggerty, R., Hinz, C., Hooper, R., Kirchner, J., Roderick, M., Selker, l., Weiler, J.M.,, 2007. Moving beyond heterogeneity and process complexity: a new vision for watershed hydrology. Water Resour. Res. 43, W07301. https://doi.org/10.1029/2006WR005467.

Moore, R.J., Clarke, R.T., 1981. A distribution function approach to rainfall–runoff modelling. Water Resour. Res. 17 (5), 1367–1382. https://doi.org/10.1029/WR017i005p01367.

Moran, M., Clarke, T., Inoue, Y., Vidal, A., 1994. Estimating cropwater deficit using the relation between surface-air temperature and spectral vegetation index. Remote Sens. Environ. 49, 246–263. https://doi.org/10.1016/0034-4257(94)90020-5.

Niu, G.-Y., Paniconi, C., Troch, P.A., Scott, R.L., Durcik, M., Zeng, X., Huxman, T., Goodrich, D.C., 2014. An integrated modelling framework of catchment-scale ecohydrological processes: 1. Model description and tests over an energy-limited watershed. Ecohydrology 7, 427–439. https://doi.org/10.1002/eco.1362.

Norman, J.M., Kustas, W.P., Humes, K.S., 1995. Source approach for estimating soil and vegetation energy fluxes in observations of directional radiometric surface temperature. Agr. Forest Metorol. 77, 263–293. https://doi.org/10.1016/0168-1923(95)02265-Y.

Ochoa-Sánchez, A., Crespo, P., Carrillo-Rojas, G., Sucozhañay, A., Célleri, R., 2019. Actual Evapotranspiration in the High Andean Grasslands: A Comparison of Measurement and Estimation Methods. Front. Earth Sci. 7, 1–16. https://doi.org/10.3389/feart.2019.00055.

Oliphant, A.J., Spronken-Smith, R.A., Sturman, A.P., 2003. Spatial variability of surface radiation fluxes in mountainous terrain. J. Appl. Meteorol. 42, 113–128. https://doi.org/10.1175/1520-0450(2003)042<0113:SVOSRF>2.0.CO;2.

Ortega-Farias, S.O., Cuenca, R.H., Ek, M., 1996. Daytime variation of sensible heat flux estimated by the bulk aerodynamic method over a grass canopy. Agric. For. Meteorol. 81, 131–143. https://doi.org/10.1016/0168-1923(95)02278-3.

Palazzi, E., Filippi, L., Von Hardenberg, J., 2017. Insights into elevation-dependent warming in the Tibetan Plateau-Himalayas from CMIP5 model simulations. J. Clim. Dyn. 48, 3991–4008. https://doi.org/10.1007/s00382-016-3316-z.

Paniconi, C., Wood, E.F., 1993. A detailed model for simulation of catchment scale subsurface hydrologic processes. Water Resour. Res. 29 (6), 1601–1620. https://doi.org/10.1029/92WR02333.

H.L. Penman Natural Evaporation from Open Water, Bare Soil and Grass Proc. Roy. Soc. London A 194 1948 S. pp. 120–145 10.1098/rspa.1948.0037.

Philipona, R., 2013. Greenhouse warming and solar brightening in and around the Alps. Int. J. Climatol. 33, 1530–1537. https://doi.org/10.1002/joc.3531.

Previati, M., Canone, D., Iurato, E., Gisolo, D., Ferrari, S., Teatini, P., Putti, M., Ferraris, S., 2020. Thorough wetting and drainage of a peat lysimeter in a climate change scenario. Hydrol. Process. 34 (5), 1269–1284. https://doi.org/10.1002/hyp.13675.

Priestley, C.H.B., Taylor, R.J., 1972. On the assessment of the surface heat flux and evaporation using large-scale parameters. Mon. Weather Rev. 100 (2), 81–92. https://doi.org/10.1175/1520-0493(1972)100<0081:OTAOSH>2.3.CO;2.

Raes, D., Steduto, P., Hsiao, T.C., Fereres, E., 2009. AquaCrop - the FAO crop model to predict yield response to water. II. Main algorithms and software description. Special issue on "Yield Response to Water: Examination of the Role of Crop Models in Predicting Water Use Efficiency''. Agron. J. 101, 438–447. https://doi.org/10.2134/agronj2008.0139s.

Raffelli, G., Previati, M., Canone, D., Gisolo, D., Bevilacqua, I., Capello, G., Biddoccu, M., Cavallo, E., Deiana, R., Cassiani, G., Ferraris, S., 2017. Local- and plot-scale Measurements of soil moisture: time and spatially resolved field techniques in plain, hill and mountain sites. Water J. 9, 706. https://doi.org/10.3390/w9090706.

Rana, G., Katerji, N., 2000. Measurement and estimation of actual evapotranspiration in the field under Mediterranean climate: A review. Eur. J. Agron. 13 (2–3), 125–153. https://doi.org/10.1016/S1161-0301(00)00070-8.

Rebora, N., Ferraris, L., von Hardenberg, J., Provenzale, A., 2006. Rainfarm: Rainfall downscaling by a filtered autoregressive model. J. Hydrometeorol. 7 (4), 724–738. https://doi.org/10.1175/JHM517.1.

Rigon, R., Bertoldi, G., Over, T., 2006. GEOtop: A distributed hydrological model with coupled water and energy budgets. J. Hydrometeorol. 7 (3), 371–388. https://doi.org/10.1175/JHM497.1.

Ritchie, J.T., 1998. In: Tsuji, G.Y., Hoogenboom, G., Thornton, P.K. (Eds.), Understanding Options for Agricultural Production. Systems Approaches for Sustainable Agricultural Development, 7. Springer, Dordrecht.

Roerink, G., Su, Z., Menenti, M., 2000. S-SEBI: A simple remote sensing algorithm to estimate the surface energy balance. Phys. Chem. Earth Pt B 25, 147–157. https://doi.org/10.1016/S1464-1909(99)00128-8.

Rogowski, A.S., 1972. Watershed physics: soil variability criteria. Water Resour. Res. 8 (4), 1015–1023. https://doi.org/10.1029/WR008i004p01015.

Reicosky, D.C., Sharratt, B.S., Ljungkull, J.E., Baker, D.G., 1983. Comparison of alfalfa evapotranspiration measured by a weighing lysimeter and a portable chamber. Agric. Meteorol. 28, 205–211. https://doi.org/10.1016/0002-1571(83)90026-2.

Rogora, M., Frate, L., Carranza, M.L., Freppaz, M., Stanisci, A., Bertani, I., Bottarin, R., Brambilla, A., Canullo, R., Carbognani, M., Cerrato, C., Chelli, S., Cremonese, E., Cutini, M., Di Musciano, M., Erschbamer, B., Godone, D., Iocchi, M., Isabellon, M., Magnani, A., Mazzola, L., Morra di Cella, U., Pauli, H., Petey, M., Petriccione, B., Porro, F., Psenner, R., Rossetti, G., Scotti, A., Sommaruga, R., Tappeiner, U., Theurillat, J.-P., Tomaselli, M., Viglietti, D., Viterbi, R., Vittoz, P., Winkler, M., Matteucci, G., 2018. Assessment of climate change effects on mountain ecosystems through across-site analysis in the Alps and Apennines. Sci. Total Environ. 624, 1429–1442.

Rottler, E., Kormann, C., Francke, T., Bronstert, A., 2019. Elevation-dependent warming in the Swiss Alps 1981–2017: Features, forcings and feedbacks. Int. J. Climatol. 39 (5), 2556–2568. https://doi.org/10.1002/joc.5970.

Schirpke, U., Kohler, M., Leitinger, G., Fontana, V., Tasser, E., Tappeiner, U., 2017. Future impacts of changing land-use and climate on ecosystem services of mountain grassland and their resilience. Ecosyst. Serv. 26, 79–94. https://doi.org/10.1016/j.ecoser.2017.06.008.

Sarkar, S., Roy, A.K., Martha, T.R., 2013. Soil depth estimation through soil-landscape modelling using regression kriging in a Himalayan terrain. Int. J. Geogr. Inf. Sci. 27, 2436–2454. https://doi.org/10.1080/13658816.2013.814780.

Schwanghart, W., Scherler, D., 2014. TopoToolbox 2 – MATLAB-based software for topographic analysis and modeling in Earth surface sciences. Earth Surf. Dyn. 2, 1–7. https://doi.org/10.5194/esurf-2-1-2014.

Sharma, V., Kilic, A., Irmak, S., 2016. Impact of scale/resolution on evapotranspiration from Landsat and MODIS images. Water Resour. Res. 52, 1800–1819. https://doi.org/10.1002/2015WR017772.

Steiger, R., 2010. The impact of climate change on ski season length and snowmaking requirements in Tyrol. Austria. Clim. Res. 43 (3), 251–262. https://doi.org/10.3354/cr00941.

Stull, R.B., 1988. Introduction to Boundary-Layer Meteorology. Kluwer Academic Publishers, Dordrecht, p. 666.

Su, Z., 2002. The Surface Energy Balance System (SEBS) for estimation of turbulent heat fluxes. Hydrol. Earth Syst. Sci. 6, 85–100. https://doi.org/10.5194/hess-6-85-2002.

Thornthwaite, C.W., 1948. An approach toward a rational classification of climate. Geogr. Rev. 38, 55–94. https://doi.org/10.2307/210739.

Tromp-van Meerveld, H., McDonnell, J., 2006. On the interrelations between topography, soil depth, soil moisture, transpiration rates and species distribution at the hillslope scale. Adv. Water Resour. 29 (2), 293–310. https://doi.org/10.1016/j.advwatres.2005.02.016.

J. Twidell T. Weir Renewable energy resources 1986 E&FN Spon London, UK 10.4324/9781315766416 160.

USGS, 2019. Landsat 8 (L8) Data Users Handbook. U.S. Geological Survey, Earth Resources Observation and Science (EROS) Center, Sioux Falls, South Dakota, pp. 114.

Van den Bergh, T., Körner, C., Hiltbrunner, E., 2018. *Alnus* shrub expansion increases evapotranspiration in the Swiss Alps. Reg. Environ. Change 18, 1375–1385. https://doi.org/10.1007/s10113-017-1246-x.

Van Looy, K., Bouma, J., Herbst, M., Koestel, J., Minasny, B., Mishra, U., Montzka, C., Nemes, A., Pachepsky, Y.A., Padarian, J., Schaap, M.G., Tóth, B., Verhoef, A., Vanderborght, J., Ploeg, M.J., Weihermüller, L., Zacharias, S., Zhang, Y., Vereecken, H., 2017. Pedotransfer functions in Earth system science: challenges and perspectives. Rev. Geophys. 55 (4), 1199–1256.

Vanham, D., 2012. The Alps under climate change: implications for water management in Europe. J. Water Clim. Chang. 3, 197–206. https://doi.org/10.2166/wcc.2012.032.

Venturini, V., Islam, S., Rodriguez, L., 2008. Estimation of evaporative fraction and evapotranspiration from MODIS products using a complementary based model. Remote Sens. Environ. 112 (1), 132–141. https://doi.org/10.1016/j.rse.2007.04.014.

Wang, K., Dickinson, R.E., 2012. A review of global terrestrial evapotranspiration: observation, climatology, and climatic variability. Rev. Geophys. 50 (2), RG2005. https://doi.org/10.1029/2011RG000373.

Wang, S., Pan, M., Mu, Q., Shi, X., Mao, J., Brümmer, C., Jassal, R.S., Krishnan, P., Li, J., Black, T.A., 2015. Comparing evapotranspiration from eddy covariance measurements, water budgets, remote sensing, and land surface models over Canada. J. Hydrometeorol. 16, 1540–1560. https://doi.org/10.1175/JHM-D-14-0189.1.

Wegehenkel, M., Beyrich, F., 2014. Modelling of hourly evapotranspiration and soil water content at the grass-covered boundary-layer field site Falkenberg. Germany. Hydrol. Sci. J. 59 (2), 376–394. https://doi.org/10.1080/02626667.2013.835488.

Wever, L.A., Flanagan, L.B., Carlson, P.J., 2002. Seasonal and interannual variation in evapotranspiration, energy balance and surface conductance in a northern temperate grassland. Agric. For. Meteorol. 112, 31–49. https://doi.org/10.1016/S0168-1923(02)00041-2.

Wösten, J.H.M., Schuren, C.H.J.E., Bouma, J., Stein, A., 1990. Functional sensitivity analysis of four methods to generate soil hydraulic functions. Soil Sci. Soc. Am. J. 54 (3), 832–836. https://doi.org/10.2136/sssaj1990.03615995005400030036x.

Whiteman, C.D., Eisenbach, S., Pospichal, B., Steinacker, R., 2004. Comparison of vertical soundings and sidewall air temperature measurements in a small alpine basin. J. Appl. Meteorol. 43 (11), 1635–1647. https://doi.org/10.1175/JAM2168.1.

Zhao, W., Li, A., 2015. A Review on Land Surface Processes Modelling over Complex Terrain. Adv. Meteorol. 17, ID607181. https://doi.org/10.1155/2015/607181.